Fermi Surface of an Important Nanosized Metastable Phase: Al_3Li

J. Laverock,[1] S. B. Dugdale,[1] M. A. Alam,[1] M. V. Roussenova,[1] J. R. Wensley,[1] J. Kwiatkowska,[2] and N. Shiotani[3]

[1]*H. H. Wills Physics Laboratory, University of Bristol, Tyndall Avenue, Bristol BS8 1TL, United Kingdom*

[2]*H. Niewodniczański Institute of Nuclear Physics, Polish Academy of Sciences, Radzikowskiego 152, 31-342 Kraków, Poland*

[3]*KEK-PF, Tsukuba, Ibaraki 305-0801, Japan*

(Received 12 September 2010; published 1 December 2010)

Nanoscale particles embedded in a metallic matrix are of considerable interest as a route towards identifying and tailoring material properties. Al-Li alloys, which form ordered nanoscale precipitates of Al_3Li for a range of concentrations, have been deployed successfully in the aerospace industry owing to their superior strength-to-weight ratio. The precipitates are metastable and their electronic structure has so far been inaccessible through conventional techniques. Here, we take advantage of the strong positron affinity of Li to probe the Fermi surface of nanoscale Al_3Li precipitates.

DOI: 10.1103/PhysRevLett.105.236401 PACS numbers: 71.18.+y, 73.22.−f, 78.70.Bj

In recent years, many of the properties of the Al-Li alloy system have come under careful scrutiny, in part because of the widespread interest in these materials by the aerospace industry. In the Al-rich region of the phase diagram (Li concentrations between 5% and 25%), these alloys offer high stiffness and superior strength-to-weight ratios, principally due to the hardening which occurs through the precipitation of nanoscale particles. The Li-rich strengthening precipitates, known as the δ' phase, are Al_3Li and are highly ordered with an $L1_2$ structure, and remain crystallographically coherent with the parent (fcc) solid-solution matrix with small lattice mismatch [1,2]. The size of the precipitates and the volume they occupy depend not only on the Li concentration, but also on the particular conditions experienced (such as heat treatment and aging) [3]; for the Al-9 at. % Li samples considered here, that volume is approximately 20%, comprising roughly spherical precipitates with an average diameter of about 20 nm.

However, the δ' phase is metastable [2], and only exists within the parent Al fcc matrix. For this reason, knowledge of the electronic structure of the Al_3Li precipitates has so far only come from band-theoretical calculations (see, for example, [4]). Although some of the strengthening qualities originate from the fact that the precipitates act as pinning centers for defects, it is believed that Al_3Li has a particularly high Young's modulus, which, of course, stems from its electronic structure [5,6].

Advantage is taken in this study of the strong positron affinity of Li-rich regions [7] to directly probe the electronic structure (in the form of its Fermi surface) of the δ'-phase Al_3Li precipitates. Here, the strong positron affinity leads to the trapping of most of the positrons in the precipitates facilitating an unambiguous probing of the properties of the precipitates alone since the experimental signatures are sufficiently different from the host matrix. Previous pioneering positron studies of nanoscale precipitates [8,9] (and even quantum dots [10]) have, for a variety of reasons, restricted their analyses to p space rather than k space. Here, the Fermi surface (FS) of the precipitate itself is the objective.

Positron annihilation is a well-established technique for investigating the occupation densities in k space, and hence the FS, which is accessed via the momentum distribution measured by the 2D angular correlation of electron-positron annihilation radiation (2D ACAR) technique [11]. A 2D ACAR measurement yields a 2D projection of the underlying electron-positron momentum density, $\rho^{2\gamma}(\mathbf{p})$, in which the FS is expressed through discontinuities in the distribution at the Fermi momenta $\mathbf{p}_F = \mathbf{k}_F + \mathbf{G}$, where $\mathbf{k}_F$ represent the loci of the FS in k space and $\mathbf{G}$ is a vector of the reciprocal lattice. When the FS is of paramount interest, the application of the Lock-Crisp-West procedure [12] is used to superimpose the contribution from successive Brillouin zones (BZ) into the first BZ, thereby directly providing a map of the projection of the occupied states in the BZ (i.e., a projection of the FS).

In order to assess the topology of the measured FS, positron annihilation (2D ACAR) measurements have been combined with *ab initio* electronic structure calculations. The aim of this combined approach is to (a) establish that the measured Fermi surface indeed arises from the precipitates alone and (b) obtain as accurate a picture as possible of the first experimental FS of the Al_3Li phase. To achieve these goals, first of all, we consider the annihilation of the positron, and, in particular, its sensitivity to the ordered precipitates, by considering all possible scenarios: (i) the positron annihilates *only* with delocalized electrons in the δ' precipitates, and our measured FS is that of $L1_2$ Al_3Li, (ii) the positron annihilates with the Al matrix, and our measured FS resembles pure Al, (iii) the positron annihilates from both the Al_3Li precipitates *and* the Al matrix, and our FS measurement is a weighted average of both, (iv) our measurements reflect the stoichiometry of the sample, and the FS resembles that of the disordered alloy $Al_{0.91}Li_{0.09}$. Electronic structure calculations of pure Al and Al_3Li have been performed using the linear

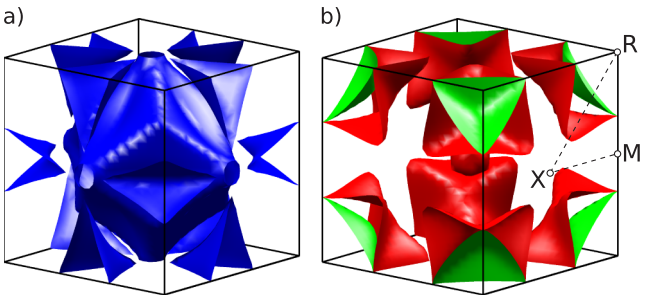

FIG. 1 (color online). The hole (a) and two electron (b) FS sheets of Al_3Li predicted by the LMTO calculation. The symmetry points of the BZ are labeled in (b); the Γ point is at the center.

muffin-tin orbital (LMTO) method [13], whereas for the disordered $Al_{0.91}Li_{0.09}$ and $Al_{0.75}Li_{0.25}$ alloys, the Korringa-Kohn-Rostoker (KKR) within the coherent potential approximation (CPA) framework [14] was employed. Full-potential calculations (using the ELK code [15]) have also been performed to investigate any inaccuracies associated with the potential shape approximations employed by the LMTO and KKR implementations. The LMTO calculations predict three FS sheets for $L1_2$ Al_3Li, shown in Fig. 1, the first of which is a hole sheet (enclosing unfilled states) and the second and third are both electron sheets (enclosing filled electron states). These calculations agree well with previous calculations [4], as well as with our KKR and ELK calculations (not presented here). Moreover, the ELK calculations yield a large (zero-temperature) Young's modulus of 137 GPa, in excellent agreement with the findings of Ref. [5].

A single crystal of the Al-Li alloy was grown by the Bridgman method from high purity Al (99.999%) and Li (99.95%) by adding Li into molten Al, followed by stirring and casting, sealed within a stainless steel capsule under an Ar pressure of 3 atm to prevent excessive loss of Li during the crystallization process. The final Li content in the single crystal was determined by atomic absorption spectrometry and independently in each sample by proton induced gamma emission and was found to be 9 at. %. The crystal was oriented using Laue backreflection, and specimens of 1.5 mm thickness were cut along planes normal to the main crystallographic directions. The usual procedure of alternate mechanical polishing and chemical polishing was applied to remove damaged surface layers. Separate measurements on the same samples of the positron lifetime [16] indicate that the positron is fully trapped in (and therefore annihilates from) the Al_3Li δ' precipitates [17], already hinting at scenario (i) outlined above.

A series of 2D ACAR measurements along four different crystallographic directions ([100], [110], [111] and [210]) were made on the Bristol spectrometer [with a resolution function of 0.16 (p_x) and 0.19 (p_y) of ($2\pi/a$)] and analyzed in order to obtain the projected electron-positron momentum density in the first BZ, shown in Fig. 2 (in the absence of positron effects, this would simply correspond to the occupation density in the first BZ). Note that the additional smearing of the FS due to confinement effects is expected to be negligible compared with the experimental resolution [18]. The sensitivity of our data to the FS is immediately obvious: Strong regions of high momentum (occupation) density are observed near the projected R points of the BZ, at which each sheet of FS is fully occupied. To accompany these measurements, the 3D electron-positron momentum density was computed from our electronic structure calculations [13] and the projected (2D) density in the first BZ was obtained for each corresponding projection.

We begin with a visual comparison of the measured quantities and their corresponding theoretical distributions. Good agreement is already observed between the data and the LMTO calculations of Al_3Li shown in Fig. 2. However, in order to eliminate the possibility that the positron is sampling the Al matrix rather than the δ' precipitates [scenario (ii)], both experimental and theoretical distributions were also obtained of pure Al along two crystallographic projections ([110] and [111]), shown in Fig. 3 in the same $L1_2$ BZ of Al_3Li. The nearly free-electron nature of the band structure of Al, leading to an almost spherical FS, is evident in Fig. 3. Unsurprisingly, good agreement is observed between experiment and theory for Al, but there are stark differences between the Al distributions and our experimental data for Al-9 at. % Li. In the [110] projection [comparing Figs. 2(c) and 3(b)], the most obvious differences are in the shape of the projected FS near RX, as well as the distribution near ΓM and X. For the [111] projection [comparing Figs. 2(c) and 3(b)], the shape of the distribution, particularly near MX, is markedly different. Linear combinations of the distributions of the pure Al and $L1_2$ Al_3Li calculations were not found to improve the agreement between experiment and theory over the Al_3Li calculations alone, eliminating scenario (iii) and further suggesting that *all* of the positrons annihilated from the Li-rich precipitates, in agreement with independent positron lifetime measurements [16].

In order to address the final alternative possibility [scenario (iv)], i.e., that the positron is sampling a *disordered* alloy of the sample stoichiometry, KKR-CPA calculations have been performed for disordered $Al_{0.91}Li_{0.09}$, and are shown in Fig. 4 for two different projections (namely [110] and [111]) in the right-hand panels. For the [110] direction of our data shown in Fig. 2(b), the lowest density is observed at X, and there is a weak peak at ΓM, a feature that is well reproduced by our LMTO calculations. In contrast, for the $Al_{0.91}Li_{0.09}$ calculation [Fig. 4(a)], the minimum density is located at ΓM, and the shape of the feature at RX is substantially different. Further inspection of the [111] projection [comparing Figs. 2(c) and 4(b)] yields similar conclusions, leading us to eliminate this scenario. Finally, we can consider the

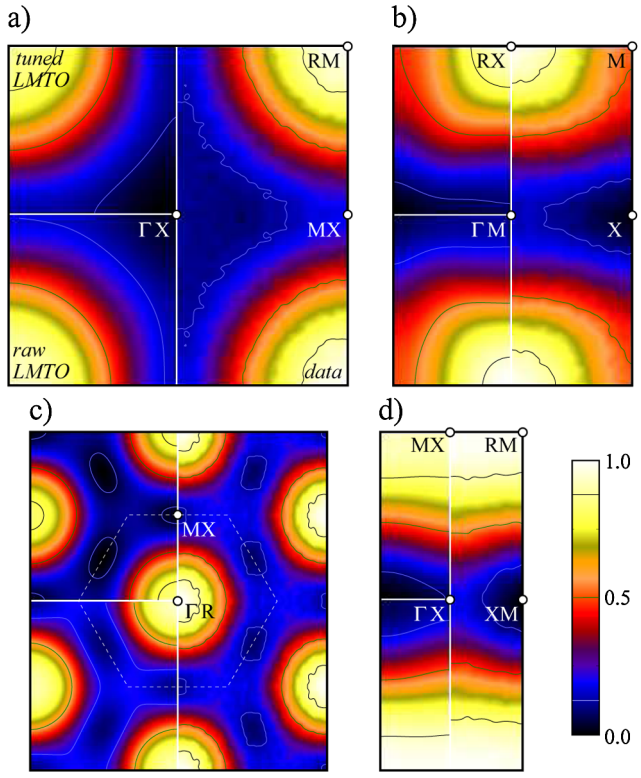

FIG. 2 (color online). Positron annihilation data in the first BZ for Al-9 at. % Li, shown in the right-hand panels, projected along the (a) [100], (b) [110], (c) [111], and (d) [210] crystallographic directions. High symmetry points have been labeled in projection.

possibility that, although the measurements are sensitive to the precipitate phase, the precipitates themselves may not be ordered. However, comparisons with a KKR-CPA calculation of disordered $Al_{0.75}Li_{0.25}$, shown in the left-hand panels of Fig. 4, although superficially similar, are quantitatively in poorer agreement with the data than the ordered Al_3Li calculations. This leads us to our first conclusion: that the positron is sampling the Li-rich δ' precipitate phase of ordered $L1_2$ Al_3Li.

In terms of the FS topology, the agreement between the data and LMTO Al_3Li calculations, although already very good, can be "tuned" by rigidly shifting the theoretical bands, culminating in a fitted FS whose overall shape more resembles the experimental FS. This approach has already been successfully applied in p space to both positron [19] and Compton scattering [20] data. Here, we operate in k space, and employ the state-dependent enhancement scheme outlined in Ref. [21]. The results of the rigid-band fit, as expected, reflect the higher positron affinity of Li over Al, with the positron preferentially annihilating from within the Li atomic sphere (34.6%) rather than the equally sized Al atomic sphere (21.8% × 3). The state-dependent enhancement factors (see Ref. [21]) demonstrate the deenhancement of p states (by a factor 0.59) and d states (by a factor 0.43) relative to the s states that has previously been observed for transition metals and semiconductors [22,23].

First, the rigid-band fit is found to be sensitive to all of the FS sheets, unambiguously confirming their presence. The bands are found to shift upwards in energy (becoming less occupied) by ~50 mRy, and lead to a tuned FS, shown in Fig. 5. It is emphasized that there are no constraints to these parameters, meaning that each sheet of FS is individually free to be completely empty or fully occupied, or indeed any shape in between allowed by its band structure. Although the shifts are quite large, the bands are of predominantly p character and have large Fermi velocities (energy gradients), and so the modification (in k space) to the Fermi breaks themselves is weaker. Indeed, we find that this shift in the Fermi wave vector is $\Delta k_F \sim 0.05 - 0.08(2\pi/a)$, which is less than half of the experimental resolution function. Nonetheless, these shifts still correspond to a total reduction in the number of occupied states of ~0.84 electrons. The most plausible interpretation of these results is that the topology of the experimental FS more closely resembles that shown in Fig. 5 than the raw LMTO calculation of Fig. 1. In previous studies, the present fitting method has been found to improve the description of the FS (in comparison with high-precision

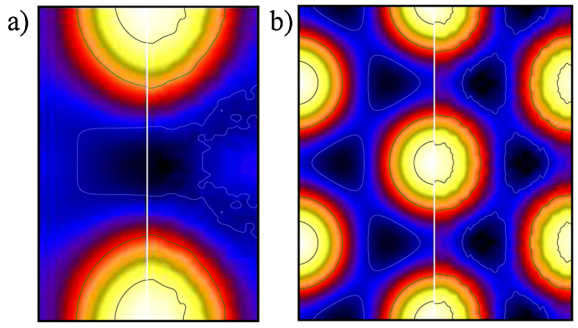

FIG. 3 (color online). LMTO (left-hand panels) and 2D ACAR data (right-hand panels) for pure Al, shown in the $L1_2$ BZ projected along the (a) [110] and (b) [111] crystallographic directions.

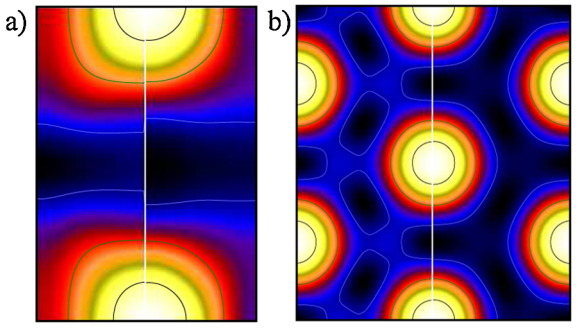

FIG. 4 (color online). KKR-CPA calculations of the momentum distribution of disordered $Al_{0.75}Li_{0.25}$ (left-hand panels) and $Al_{0.91}Li_{0.09}$ (right-hand panels) projected along the (a) [110] and (b) [111] directions.

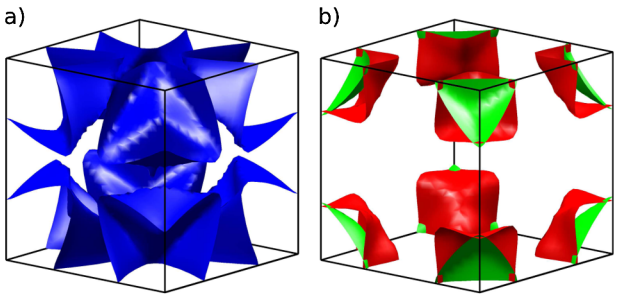

FIG. 5 (color online). The FS obtained by tuning our LMTO calculation of Al_3Li to the experimental data (compare with Fig. 1). Note that the rigid-band nature of the fitting procedure places no constraints on the Fermi volume (see text for details).

quantum oscillation measurements) in all the systems investigated (including Al) [21]. Moreover, the LDA is well known to place the d bands (unoccupied in Al_3Li) too low with respect to sp bands in transition metals [24]. Our raw LMTO calculations of Al_3Li predict an appreciable hybridization with these unoccupied d states, having 26% total d character at E_F. In the rigid-band fit, however, this quantity is somewhat reduced, as the sp bands below E_F and d bands above E_F are pushed apart. The results of the fit can be interpreted as a reaction to the overestimation by the LDA of the hybridization between the sp and d states, where the flatter d bands, overestimated at E_F, impact on the topology of the FS. Since the computation of the elastic constants can only be performed at the minimum of the LDA, the impact these results might have on the predicted material properties of Al_3Li (such as its Young's modulus) remains open to investigation.

In summary, we have successfully measured the FS of a nanosized metastable phase of matter, previously inaccessible using conventional techniques. By taking advantage of the positron affinity of Li, our 2D ACAR measurements of Al-9 at. % Li yield a momentum density in close agreement with electronic structure calculations of ordered $L1_2$ Al_3Li, corresponding to the δ' precipitates. Moreover, comparisons with theoretical distributions of pure Al as well as of the disordered alloys $Al_{0.91}Li_{0.09}$ and $Al_{0.75}Li_{0.25}$ eliminate other plausible fates of the positron, firmly establishing the positron as a unique probe of the δ' precipitates. Detailed subsequent analysis of the momentum density has yielded a tuned FS for this elusive phase.

[1] B. Noble and G. E. Thompson, Met. Sci. **5**, 114 (1971); S. F. Baumann and D. B. Williams, Scr. Metall. **18**, 611 (1984); K. Mahalingham *et al.*, Acta Metall. **35**, 483 (1987).
[2] M. Sluiter *et al.*, Phys. Rev. B **42**, 10460 (1990).
[3] M. E. Krug, D. C. Dunand, and D. N. Seidman, Appl. Phys. Lett. **92**, 124107 (2008); V. Radmilovic *et al.*, Scr. Mater. **58**, 529 (2008).
[4] X.-Q. Guo *et al.*, Phys. Rev. B **41**, 12 432 (1990).
[5] X.-Q. Guo, R. Podloucky, and A. J. Freeman, J. Mater. Res. **6**, 324 (1991).
[6] A. Mikkelsen *et al.*, Phys. Rev. Lett. **87**, 096102 (2001).
[7] M. J. Puska, P. Lanki, and R. M. Niemenen, J. Phys. Condens. Matter **1**, 6081 (1989).
[8] Y. Nagai *et al.*, Phys. Rev. Lett. **87**, 176402 (2001); Y. Nagai *et al.*, Phys. Rev. B **79**, 201405(R) (2009).
[9] P. Asoka-Kumar *et al.*, Philos. Mag. Lett. **82**, 609 (2002).
[10] S. W. H. Eijt *et al.*, Nature Mater. **5**, 23 (2006).
[11] R. N. West, in *Positron Spectroscopy of Solids*, Proceedings of the International School of Physics "Enrico Fermi," Course CXXV, edited by A. Dupasquier and A. P. Mills, Jr. (IOS, Amsterdam, 1995), p. 75.
[12] D. G. Lock, V. H. C. Crisp and R. N. West, J. Phys. F **3**, 561 (1973).
[13] B. Barbiellini, S. B. Dugdale, and T. Jarlborg, Comput. Mater. Sci. **28**, 287 (2003).
[14] H. Ebert, *Electronic Structure and Physical Properties of Solids*, edited by H. Dreyssé, Lecture Notes in Physics Vol. 535 (Springer, Berlin 1998), p. 191; http://olymp.cup.uni-muenchen.de/ak/ebert/SPRKKR/.
[15] J. K. Dewhurst *et al.*, http://elk.sourceforge.net.
[16] The lifetime measurements were performed by J. Dryzek.
[17] J. Del Río, F. Plazaola, and N. De Diego, Philos. Mag. A **69**, 591 (1994).
[18] Z. Tang *et al.*, J. Phys. Condens. Matter **20**, 445203 (2008).
[19] Zs. Major *et al.*, Phys. Rev. Lett. **92**, 107003 (2004); Zs. Major *et al.*, J. Phys. Chem. Solids **65**, 2011 (2004).
[20] C. Utfeld *et al.*, Phys. Rev. Lett. **103**, 226403 (2009); C. Utfeld *et al.*, Phys. Rev. B **81**, 064509 (2010).
[21] J. Laverock *et al.*, Phys. Rev. B **82**, 125127 (2010).
[22] T. Jarlborg and A. K. Singh, Phys. Rev. B **36**, 4660 (1987).
[23] B. Barbiellini *et al.*, Phys. Rev. B **56**, 7136 (1997).
[24] S. Wakoh and J. Yamashita, J. Phys. Soc. Jpn. **35**, 1394 (1973); H. Eckardt, L. Fritsche, and J. Noffke, J. Phys. F **14**, 97 (1984).